molecules

MDPI

Article

# Luminescent κ-Carrageenan-Based Electrolytes Containing Neodymium Triflate

**S. C. Nunes [1,2,*], S. M. Saraiva [1], R. F. P. Pereira [3], M. M. Silva [3], L. D. Carlos [4], P. Almeida [2,5], M. C. Gonçalves [1,6], R. A. S. Ferreira [4] and V. de Zea Bermudez [1,6,*]**

1 Chemistry Department, University of Trás-os-Montes e Alto Douro, 5001-801 Vila Real, Portugal; sofia.m.s.73@gmail.com (S.M.S.); cristina@utad.pt (M.C.G.)
2 Chemistry Department, University of Beira Interior, 6201-001 Covilhã, Portugal; pjsa@ubi.pt
3 Chemistry Department, University of Minho, 4710-057 Braga, Portugal; rpereira@quimica.uminho.pt (R.F.P.P.); nini@quimica.uminho.pt (M.M.S.)
4 Physics Department, University of Aveiro, 3810-193 Aveiro, Portugal; lcarlos@ua.pt (L.D.C.); rferreira@ua.pt (R.A.S.F.)
5 CICS-UBI, University of Beira Interior, 6201-001 Covilhã, Portugal
6 CQ-VR, University of Trás-os-Montes e Alto Douro, 5001-801 Vila Real, Portugal
* Correspondence: snunes@ubi.pt (S.C.N.); vbermude@utad.pt (V.d.Z.B.); Tel.: +351-259-350000 (V.d.Z.B.)

Received: 13 February 2019; Accepted: 8 March 2019; Published: 14 March 2019


**Abstract:** In recent years, the synthesis of polymer electrolyte systems derived from biopolymers for the development of sustainable green electrochemical devices has attracted great attention. Here electrolytes based on the red seaweeds-derived polysaccharide κ-carrageenan (κ-Cg) doped with neodymium triflate ($NdTrif_3$) and glycerol (Gly) were obtained by means of a simple, clean, fast, and low-cost procedure. The aim was to produce near-infrared (NIR)-emitting materials with improved thermal and mechanical properties, and enhanced ionic conductivity. Cg has a particular interest, due to the fact that it is a renewable, cost-effective natural polymer and has the ability of gelling in the presence of certain alkali- and alkaline-earth metal cations, being good candidates as host matrices for accommodating guest cations. The as-synthesised κ-Cg-based membranes are semi-crystalline, reveal essentially a homogeneous texture, and exhibit ionic conductivity values 1–2 orders of magnitude higher than those of the κ-Cg matrix. A maximum ionic conductivity was achieved for 50 wt.% Gly/κ-Cg and 20 wt.% $NdTrif_3$/κ-Cg ($1.03 \times 10^{-4}$, $3.03 \times 10^{-4}$, and $1.69 \times 10^{-4}$ S cm$^{-1}$ at 30, 60, and 97 °C, respectively). The NdTrif-based κ-Cg membranes are multi-wavelength emitters from the ultraviolet (UV)/visible to the NIR regions, due to the κ-Cg intrinsic emission and to $Nd^{3+}$, $^4F_{3/2} \rightarrow {}^4I_{11/2\text{-}9/2}$.

**Keywords:** κ-carrageenan; structure; biopolymer electrolyte; thermal properties; ionic conductivity; luminescence features

## 1. Introduction

The studies of solid polymer electrolytes (SPEs) based on biopolymers [1] have exponentially increased in the last few years because of the desirable properties of these macromolecules and of the growing global environmental concerns. Biopolymers offer a wide range of benefits as they are biodegradable, renewable, abundant, and non-hazardous compared to synthetic polymers. Innovative SPEs based on cellulose and its derivatives [2–4], deoxyribonucleic acid (DNA) [5,6], gelatin [7–9], chitosan [10,11], corn starch [12,13], agar [14,15], xanthan gum [16] and silk fibroin [17], were introduced. In the same context, we explored the use of the red-seaweeds-derived carrageenan (Cg) acid polysaccharides [18]. All these works revealed that these natural macromolecules have tremendous application potential [19] in various solid state electrochemical devices such as

dye-sensitized solar cells [20,21], fuel cells [22–24], energy storage devices [3], and electrochromic devices (ECDs) [7,10,14].

Although Cgs are of the utmost interest for the energy area, the number of works reported in literature dealing with their use as SPEs is scarce [18,21,24–31]. Cgs are linear high-molecular-weight sulfated polysaccharides made up of repeating galactose units and 3,6-anhydrogalactose, both sulfated and non-sulfated [32], joined by alternating alpha 1-3 and beta 1-4 glycosidic linkages. They are water-soluble polymers extensively employed in the food industry sector, as stabilizer, thickener, emulsifier, and gelling agent. Cgs are composed of long, highly flexible molecules that curl, forming helical structures, and therefore, they have an ability to form a variety of different gels at room temperature. Depending on the method and the algae from which Cg is extracted, three main types of Cgs can be obtained: (1) Kappa (κ) (Figure 1a), that forms strong, rigid gels in the presence of potassium ($K^+$) ions; (2) Iota (τ) which forms soft gels in the presence of calcium ($Ca^{2+}$) ions; and (3) lambda (λ), which does not form gels. The primary differences that influence the gel properties of κ-Cg, τ-Cg and λ-*Cg* are the number and position of the ester sulfate groups in the repeating galactose units. The Cgs are all soluble in water, but, while λ-Cg forms viscous solutions, κ- and τ-Cgs form thermoreversible gels. In solution, the molecules of the κ and τ types undergo a thermoreversible coil-to-helix transition, where the helices self-associate via hydrogen bonds and ionic interactions, giving rise to a three-dimensional gel structure [33,34], which ultimately results in the formation of ionotropic and thermotropic gels [35,36]. The three-dimensional ordered packing of κ-Cg allows each sulfate group to be effectively surrounded by $K^+$ ions, forming firm, but brittle gels, [37] while τ-Cg gelation is dependent on the presence of $Ca^{2+}$ ions, forming soft and elastic gels [36]. κ-Cg can also form cross-linking networks with other components present in the SPEs, such as ionic liquids (ILs) [18] and lanthanide ions [30].

In 2017 we introduced κ-Cg-based biopolymer electrolytes with foreseen application in solid state electrochemical devices, as long as their operation does not require the flow of gases and does not lead to water formation, such as ECDs [18]. These attractive green flexible electrolytes were prepared in aqueous solution, by means of a simple, clean, fast and low-cost procedure, from κ-Cg, the IL 1-butyl-3-methylimidazolium chloride ([Bmim]Cl), and glycerol (Gly). The highest ionic conductivity achieved was $8.47 \times 10^{-4}/2.45 \times 10^{-3}$ S cm$^{-1}$ at 20/66 °C under anhydrous conditions, and 54.9/186 m S cm$^{-1}$ at 30/60 °C at a relative humidity of 98%.

More recently, we investigated a 5-layer configuration ECD including (as an external layer) amorphous indium zinc oxide (a-IZO), a conducting oxide with high transmission in the visible and near-infrared (NIR) spectral regions, together with an innovative NIR-emitting electrolyte composed of κ-Cg, Gly and erbium triflate ($ErTrif_3.xH_2O$) [30]. The sample with highest ionic conductivity ($1.5 \times 10^{-4}$ S cm$^{-1}$ at 20 °C) displayed ultraviolet (UV)/blue and NIR emissions associated with the κ-Cg based host and the $Er^{3+}$ ions ($^4I_{15/2} \rightarrow {}^4I_{13/2}$), respectively. The ECD tested demonstrated fast switching time (50 s), high switching efficiency (transmittance variations of 46/51% at 550/1000 nm), high optical density (0.89/0.75 at 550/1000 nm), outstanding coloration efficiency (450th cycle: −15,902/−13,400 cm$^2$ C$^{-1}$ and +3072/+2589 cm$^2$ C$^{-1}$ at 550/1000 nm for coloration and bleaching, respectively), excellent electrochemical stability, and self-healing following mechanical stress. The ECD encompassed two voltage-operated modes: semi-bright warm (+3.0 V, transmittances of 52/61% at 550/1000 nm) and dark cold (−3.0 V, transmittances of 7/11% at 550/1000 nm) [30].

In the present work, we enlarged the study of the NIR-emitting κ-Cg electrolytes to the analogue system doped with trivalent neodymium ($Nd^{3+}$) ions, introduced as neodymium (III) triflate ($NdTrif_3$) (Figure 1b). The $Nd^{3+}$ ions are attractive in the area of SPEs owing to their high Lewis acidity and coordination number. Silva et al. prepared SPEs from poly(oxyethylene) (POE) and europium ($Eu^{3+}$), $Nd^{3+}$, and $Er^{3+}$ triflates [38–40]. These authors reported relatively higher ionic conductivity for the system doped with $NdTrif_3$ with respect to the analogue electrolytes doped with the other two lanthanide triflates [40]. As κ-Cg exhibits relatively low ionic conductivities at room temperature (in the range of $10^{-7}$ S cm$^{-1}$ [18]), the addition of Gly and $NdTrif_3$ allowed circumventing this problem.

The surface morphology of the films was characterized by Scanning Electronic Microscopy (SEM), the structure of the films was examined by X-ray diffraction (XRD) measurements, and the thermal behavior of the films was analyzed by Differential Scanning Calorimetry (DSC). The influence of the neodymium salt concentration on the ionic conductivity values was evaluated by impedance spectroscopy. The degree of ionic association in the materials was analyzed through Fourier Transform Raman (FT-Raman) spectroscopy. The emission and excitation features were examined from the UV/visible to the NIR regions. The produced membranes were denoted as $CG_xNd_z$, where C represents κ-Cg, G stands for Gly, and x and z indicate the concentrations of Gly and $NdTrif_3$, respectively, with respect to κ-Cg.

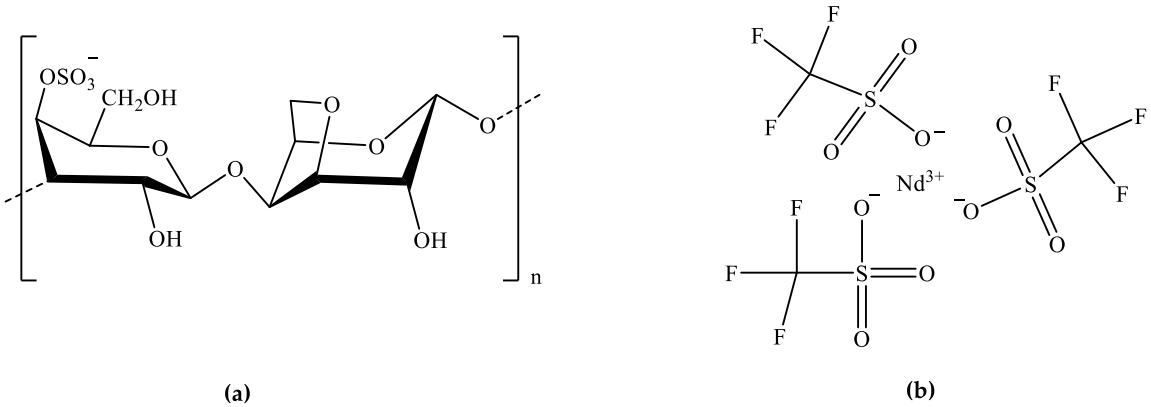


**Figure 1.** Representation of the chemical structures of κ-carrageenan (κ-Cg) (**a**) and $NdTrif_3$ (**b**).

## 2. Results and Discussion

### *2.1. Structure and Morphology*

The XRD patterns of the $CG_xNd_z$ membranes display an intense broad and non-resolved Gaussian peak located at 20.7–21.1° and weak peaks around 15.8, 18.3, 29.5 and 31.7° (Figure 2), revealing a semi-crystalline nature, with predominance of amorphous phase. In all the diffractograms of the $Nd^{3+}$-doped κ-Cg-based membranes the sharp Bragg reflections of the pure salt are missing (Figure 2, pink line), meaning that the κ-Cg-membrane is a good matrix for the dissolution and thus encapsulation of the salt in the range of concentrations analysed.

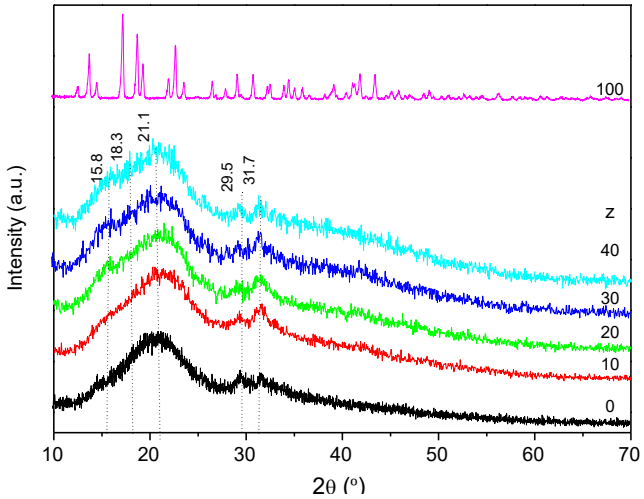


**Figure 2.** XRD curves of the non-doped (black line) and doped $CG_{50}Nd_z$ membranes, and of $NdTrif_3$ (pink line).

Carrageenan gels possess thermo-reversible property, presenting somewhat crystalline regions, called junction zones, and amorphous regions. Prior to discussing the SEM data, it is useful to explain the gelation of κ-Cg in aqueous solutions during cooling by means of the zipper model [41–44]. In light of this methodology, the gelation process can be explained through two stages: (1) the polymer chains change from random coils to helices yielding clusters soluble; and (2) rigid ordered double helices are formed which then aggregate into network junctions in the presence of the so-called gelling cations, such as $K^+$ and $Ca^{2+}$, which are responsible for the occurrence of intra- and intermolecular interactions, respectively [41–43].

Thus, the gel-sol/sol-gel transition associated with heating/cooling corresponds to the opening/closing of zippers. In addition, the crystallinity degree of κ-Cg is correlated with the degree of packing of the helices [44]. Recently, we concluded that the $CG_{50}Er_0$ membrane contained micro-aggregates of variable shapes rich in intra- and intermolecular bridges (i.e., $OSO_3^- \cdots K^+ \cdots O$ and $OSO_3^- \cdots Ca^{2+} \cdots {}^-O_3SO$ cross-linkages, respectively) [30].

The SEM images of the $CG_{50}Nd_z$ system (Figure 3) reveal that the samples display globally a homogeneous, non-rough texture. Small spherical micro-aggregates are detected in the membranes with z = 10 and 40. The analysis of the EDS mapping images of $CG_{50}Nd_z$ demonstrates that the different atoms are homogeneously distributed (Figure 3a and Figure S1, Supplementary Information). In the case of the analogue system incorporating $ErTrif_3$, the formation of larger micro-aggregates made the detection of $Ca^{2+}$, $Er^{3+}$ and $-OSO_3^-$ ions possible, thus indicating the co-existence of $[OSO_3^- \cdots Ca^{2+} \cdots {}^-O_3SO]$ and $[OSO_3^- \cdots Er^{3+} \cdots {}^-O_3SO]^+$ intermolecular cross-linkages, the latter probably counter-balanced by the $Trif^-$ ions [30]. The same applies here to the $[OSO_3^- \cdots K^+ \cdots {}^-O_3SO]$-intramolecular bridges, which are not discerned either [30]. We recall that the commercial κ-Cg employed to synthesize the $CG_{50}Nd_z$ membranes contains a minor content of $Ca^{2+}$ and $K^+$ gelling ions (see Materials in Experimental section).

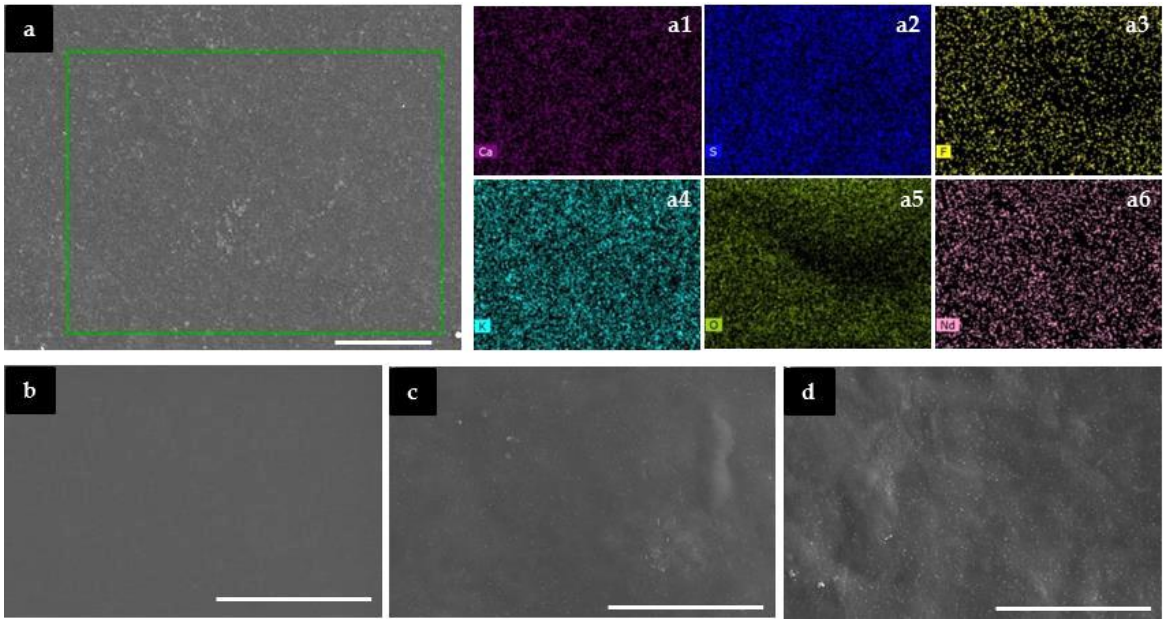


**Figure 3.** SEM images of the $CG_{50}Ndz$ membranes with z = 10% (**a**), 20% (**b**), 30% (**c**) and 40% (**d**). Scale bars = 50 μm. **a1**–**a6**: EDS mapping of the inset region of **a**.

## 2.2. Thermal Behavior

The DSC curves of the $CG_{50}Nd_z$ membranes in the 25–300 °C range, reproduced in Figure 4, show an endothermic peak centered around 123–131 °C. This event is attributed to the reversible gel-sol transition temperature ($T_{g\text{-}s}$) involving the change of the polymer chains from double helices, then to helices (soluble clusters) and ultimately to random coils. The increase of the $T_{g\text{-}s}$ of $CG_0Nd_0$

(115.0 °C) observed upon introduction of Gly and $NdTrif_3$ can be interpreted as decrease in segmental motion due to the formation of a hydrogen-bonded network between the -OH groups of Gly and the -OH and/or -C-O-C- and/or $-OSO_3^-$ polar groups of κ-Cg, and intermolecular bridges between the $Nd^+$ ions and κ-Cg, which strengthen the gel. The polymer chains become harder since the rotation of the polymer segments is blocked by these cross-linkage bonds, and the flexibility of the polymer backbone is reduced. This upshift can also be explained on the basis of the zipper model. According to this model, the heat capacity of a gel depends on the number of zippers (N), on the number of parallel links (N) of a zipper, on the rotational freedom (G) of a link, and on the energy required to open a link [42]. Consequently, the $T_{g\text{-}s}$ increase observed upon addition of $NdTrif_3$ to the host κ-Cg can be associated with an increase of N and reduction of G, as a result of the aggregation of adjacent κ-Cg double helices via the $Nd^{3+}$ ions which play the role of cross-linking agents, in a way similar to the $Ca^{2+}$ ions. However, the $T_{g\text{-}s}$ value of the various $Nd^{3+}$-doped membranes remained practically unchanged (Table 1 and Figure 4). The reason for this effect could be the occurrence of a high number of intermolecular cross-linkages all over the materials leading to the formation of many separate junction zones each involving a few double helices. This process would yield small micro-aggregates, as suggested by the SEM data.

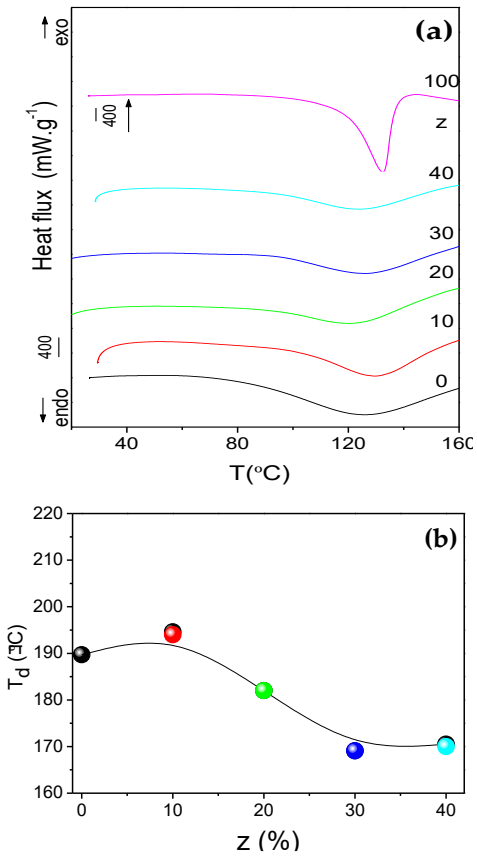


**Figure 4.** Differential Scanning Calorimetry (DSC) curves (**a**) and variation of the decomposition temperature ($T_d$) with salt content z (**b**) of the non-doped and doped $CG_{50}Nd_z$ membranes and of $NdTrif_3$ (green line). The line drawn in (**b**) is a guide for the eyes.

All the DSC curves also present an exothermic peak above 190 °C (Figure S2 of Supporting Information and Table 1) associated with the thermal decomposition ($T_d$) of the κ-Cg [18]. The analysis of Figure 4b leads us to conclude that doping the $CG_{50}Nd_z$ matrix with low contents of $NdTrif_3$ increased the stability of the biopolymer matrix. However, the increase of $NdTrif_3$ content for $z \geq 20$ destabilized the system, shifting the onset of degradation to lower temperatures.

**Table 1.** Gel-sol transition temperature ($T_{g\text{-}s}$) and decomposition temperature ($T_d$) of the $CG_{50}Nd_z$ membranes.

| Sample | z (%) | $T_{g\text{-}s}$ (°C) | $T_d$ (°C) |
|---|---|---|---|
| κ-Cg | - | 139 [18] | 188 [18] |
| $CG_0Nd_0$ | 0 | 115 [18] | 197 [18] |
| $CG_{50}Nd_0$ | 0 | 124 | 190 |
| $CG_{50}Nd_{10}$ | 10 | 131 | 195 |
| $CG_{50}Nd_{20}$ | 20 | 124 | 182 |
| $CG_{50}Nd_{30}$ | 30 | 129 | 169 |
| $CG_{50}Nd_{40}$ | 40 | 124 | 170 |

### *2.3. Ionic Conductivity Study*

The degree of salt dissociation, salt concentration, ion mobility, the dielectric constant of the host polymer, and the segmental mobility of the polymer chains [45,46] influence the ion transport properties of SPEs. In the present work, Gly was added as plasticizer to increase the amorphous phase content; dissociate ionic aggregates, and lower the glass transition temperature [45] of the $CG_{50}Ndz$ membranes.

Figure 5 shows the Arrhenius conductivity plot of the $CG_{50}Nd_z$ membranes in the 20–110 °C temperature range at variable concentration of $NdTrif_3$. Below the $T_{g\text{-}s}$ value all the doped samples demonstrate a non-linear variation of the ionic conductivity with temperature, a behavior typically found in disordered electrolytes. This process is favoured in the presence of the plasticizer which primarily increases the fraction of free volume by better separation of the polymer chains and ultimately influences the movement of charge carriers. The examination of this plot reveals that the membrane with the highest conductivity in the temperature range studied is $CG_{50}Nd_{20}$. This sample exhibits $1.03 \times 10^{-4}$, $3.03 \times 10^{-4}$, and $1.69 \times 10^{-4}$ S cm$^{-1}$ at 30, 60, and 97 °C, respectively (Figure 5, green symbols). With the increase of salt content (z = 30), a marked reduction in conductivity is observed (Figure 5, blue symbols). At this salt composition the salt begins to be poorly dissociated and ion aggregates probably form. As a consequence, the number and mobility of charged species present in the electrolyte system is reduced at high salt content and hence the conductivity decreases. However, at z = 40 the ionic conductivity suffers a slight increase. We will return to the analysis of the concentration dependence of conductivity in the section devoted to the FT-Raman analysis. Above the $T_{g\text{-}s}$ value the ionic conductivity of most samples suffered a marked decrease. This effect can be ascribed to the dramatic loss of the mechanical properties of the membranes at temperatures higher than $T_{g\text{-}s}$.

It is worth comparing the present results with those reported elsewhere for $CG_{50}Er_z$ electrolytes [30] and POE/$Nd^{3+}$ [40]. The conductivity values of the present system are similar to those reported for SPEs based on κ-Cg and $ErTrif_3$ ($1.5 \times 10^{-4}$ and $3.6 \times 10^{-4}$ S cm$^{-1}$ at 20 and 60 °C, respectively) [30], or POE and $NdTrif_3$ ($3.16 \times 10^{-4}$ S cm$^{-1}$ at 30 °C) [40].

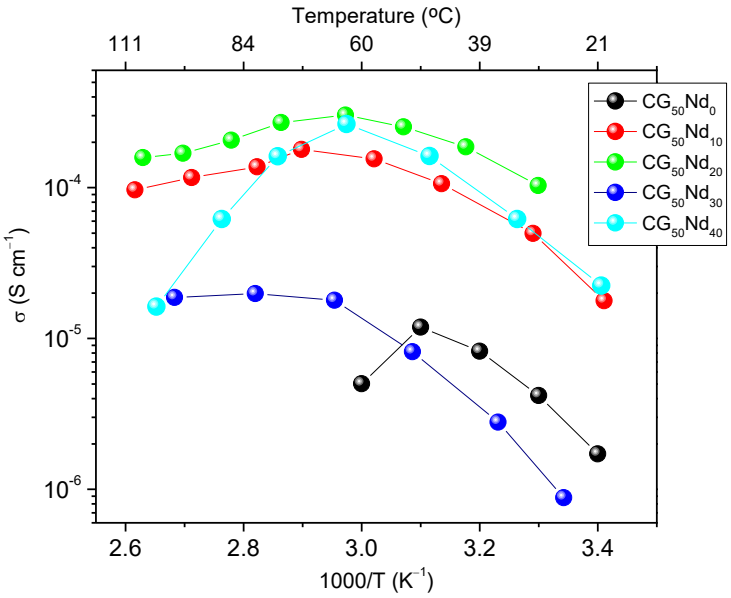


**Figure 5.** Arrhenius conductivity plot of the $CG_{50}Nd_z$ membranes.

### *2.4. Ionic Association Study*

To evaluate the ionic association in the $Nd^{3+}$-doped κ-Cg-based membranes, the symmetric stretching vibration mode of the $SO_3$ group ($\nu_sSO_3$) was studied through the analysis of the FT-Raman spectra. Several species are known to exist in SPEs: (a) "free" or weakly bonded ions with considerable mobility; (b) cations strongly bonded to the host polymer and thus with low mobility; (c) ionic aggregates, such as contact ion pairs and higher ionic multiplets, with low-moderate mobility.

The FT-Raman spectra of the $CG_{50}Nd_z$ membranes in the $\nu_sSO_3$ region is represented in Figure 6a. Because the $\nu_sSO_3$ band is superimposed with that due to the stretching vibration mode of the S=O group of the sulfate ester (-$OSO_3H$ unit) of κ-Cg, at 1063 cm$^{-1}$ [47], it was necessary to first subtract the FT-Raman spectrum of the matrix from those of the $Nd^{3+}$-doped κ-Cg-based membranes. Figure 6b shows the results of the curve-fitting performed in the subtracted $\nu_sSO_3$ FT-Raman band.

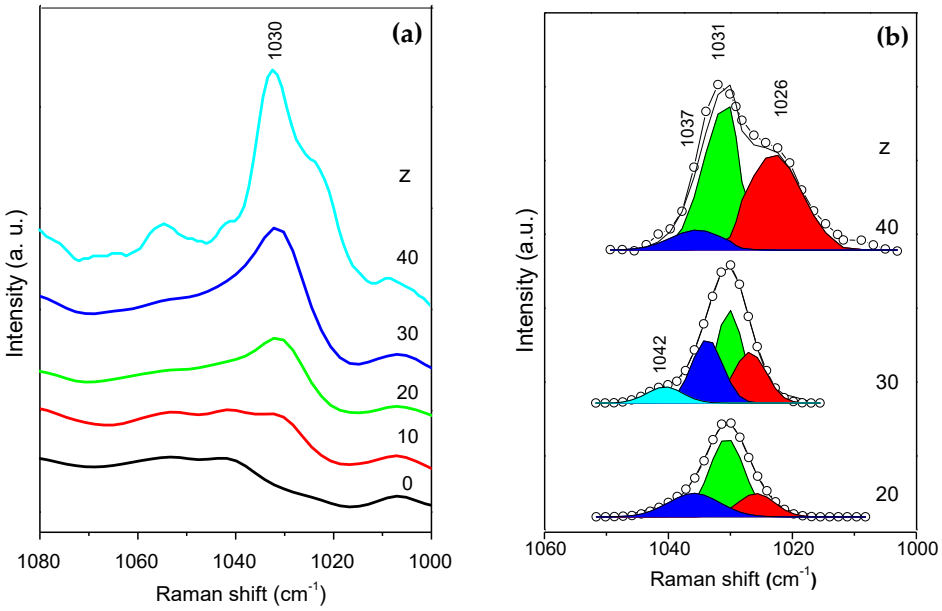


**Figure 6.** FT-Raman spectra (**a**) and curve-fitting results performed with the subtrated FT-Raman spectra (**b**) of the $CG_{50}Nd_z$ membranes in the $\nu_sSO_3$ region.

In short, the $\nu_s SO_3$ FT-Raman band of the $CG_{50}Nd_z$ membranes with $z \leq 20\%$ was resolved into three components: a sharp band at 1031 $cm^{-1}$ assigned to "free" ions and two shoulders around 1037 and 1026 $cm^{-1}$ (Figure 6b), attributed to weakly coordinated triflate ions located in two different anionic environments [48]. In the $CG_{50}Nd_{30}$ membrane, a new component at 1042 $cm^{-1}$ emerges (Figure 5b). This component is tentatively attributed to the formation of a crystalline compound of unknown composition and stoichiometry [48]. The presence of a crystalline complex in $CG_{50}Nd_{30}$ could be the reason for the drop of ionic conductivity in this membrane. In the case of the sample with z = 40, this component is not detected, but the concentration of species which produce the 1026 $cm^{-1}$ band is much higher. This might explain the higher ionic conductivity of this electrolyte with respect to $CG_{50}Nd_{30}$. The spectroscopic analysis carried out provides evidence that, as expected, some of the charge carriers of membrane with highest conductivity ($CG_{50}Nd_{20}$) are very likely "free" $Trif^-$ ions or weakly coordinated species.

### *2.5. UV/Visible and NIR Analysis*

The κ-Cg-based membranes are multi-wavelength emitters from the UV/visible to the NIR region, as demonstrated in Figure 7a,b for two selected samples. The emission results from the overlap of a series of NIR straight lines ascribed to the $Nd^{3+}$, $^4F_{3/2} \rightarrow {}^4I_{11/2\text{-}9/2}$ transitions with a broad band in the UV/visible spectral region attributed to the κ-Cg intrinsic emission [49], whose emission peak position deviates to the red as the excitation wavelength increases. The emission energy dependence on the excitation wavelength indicates a large distribution of emitting centres, in good agreement with the amorphous local structure of k-Cg evidenced by XRD (Figure 2). The excitation spectra were monitored around the $Nd^{3+}$ most intense transition revealing a broad band peaking at 350 nm and a series of low-relative intensity intra-4*f* $^3$ lines arising from transitions between the $^4I_{9/2}$ excited state and the $^4D_{5/2\text{-}1/2}$, $^2I_{11/2}$, $^2L_{15/2}$, $^4G_{11/2\text{-}5/2}$, $^2G_{9/2\text{-}7/2}$, $^2K_{13/2}$, $^4S_{3/2}$ and $^4F_{7/2}$ levels. We note that an analogous broad band around 350 nm also dominates the excitation spectrum monitored within the κ-Cg intrinsic emission, despite the presence of a low-relative intensity one in the low-wavelength region. The presence of the more intense excitation band found in the excitation spectra monitored within the host emission than in that monitored within the $Nd^{3+}$ levels points out the occurrence of effective κ Cg-to-$Nd^{3+}$ energy transfer. The fact that the κ-Cg-related band is more intense than those of the intra-4*f* $^3$ transitions in the excitation spectra monitored around the $Nd^{3+}$ emission, readily indicates that the ions' excited states are mainly populated though the ligands sensitisation rather than by direct intra-$4f^3$ excitation. Moreover, the observation in the excitation spectra of Figure 7c,d of self-absorptions in the κ-Cg emission indicates the presence of κ-Cg-to-$Nd^{3+}$ radiative energy transfer, i.e., the κ-Cg emission resonant with the $Nd^{3+}$ intra-4f lines is absorbed by the metal ions and, subsequently, converted into f–f emission. Such radiative energy transfer was previously observed in $Nd^{+3}$ and received the designation of "inner filter" effect [50].

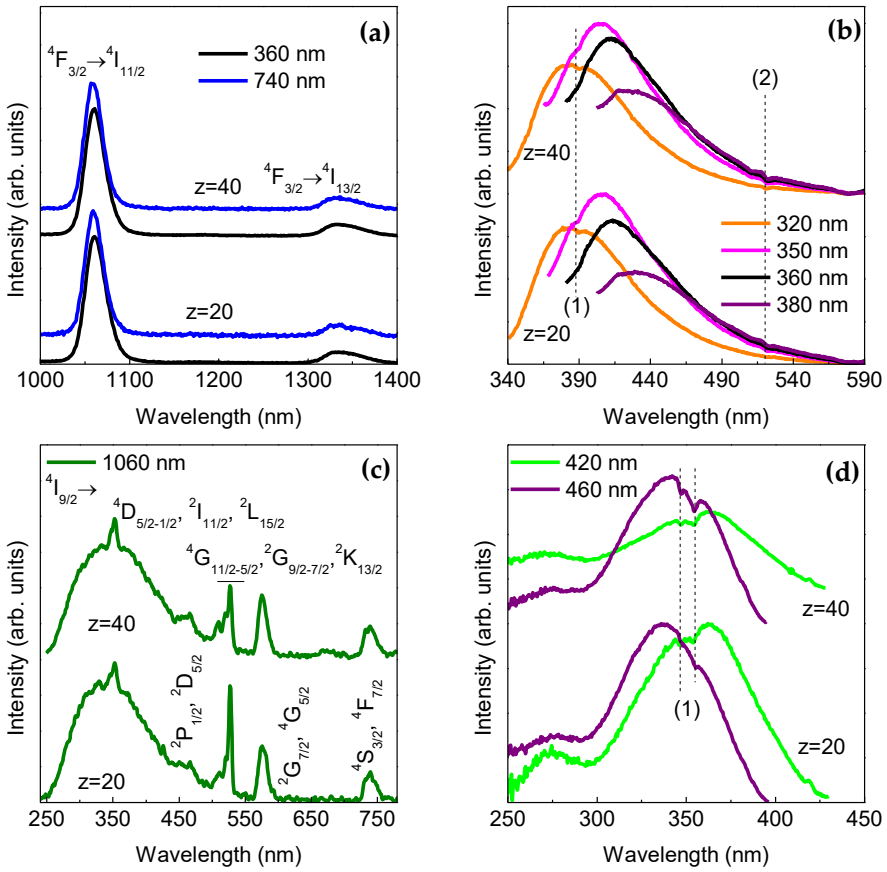


**Figure 7.** Room temperature (**a**) NIR and (b) UV/visible emission spectra and (**c**,**d**) excitation spectra of $CG_{50}Nd_z$, z = 20 and 40. The (**a**,**b**) excitation and (**c**,**d**) monitoring wavelengths are indicated in the figures. (1) and (2) denote the self-absorptions. $^4I_{9/2}\rightarrow{}^4D_{5/2\text{-}1/2}$, $^2I_{11/2}$, $^2L_{15/2}$ $^4D_{5/2\text{-}1/2}$, $^2I_{11/2}$, $^2L_{15/2}$, and $^4I_{9/2}\rightarrow{}^4G_{11/2\text{-}5/2}$, $^2G_{9/2,7/2}$, $^2K_{13/2}$, respectively.

## 3. Experimental Section

### *3.1. Materials*

κ-Cg (Carrageenan CG-130, Genugel, CP Kelco, 3 and 1.3 wt.% of $K^+$ and $Ca^{2+}$, respectively) [51], neodymium (III) triflate (NdTrif, Aldrich, Steinheim, Germany, 98%), and glycerol (Gly, Sigma-Aldrich, Steinheim, Germany, 99%) were used as received. High purity deionized water ($H_2O$) (type II pure water, using Elix Reference Water Purification System 10 from Millipore, Rephile Bioscience, Lda., Boston, MA, USA) was used in all experiments.

### *3.2. Preparation of the κ-Cg -Based Electrolytes*

A mass of approximately 0.30 g of κ-Cg was dispersed in 15 mL of distilled water and heated under magnetic stirring at 60–70 °C during 1 h for complete dissolution. A volume of 122 μL of Gly (corresponding to 50% wt. Gly/κ-Cg) and different amounts of $NdTrif_3$ were then added to this solution under stirring (Table 2). When the solutions became homogeneous, they were transferred to Petri plates and cooled down to room temperature. All the membranes prepared were stored in an oven at 50 °C over 4 days. Under these drying conditions, the colour of κ-Cg does not tend to turn brown and not observed cleavage of the glycosidic linkage [52]. The main problem associated with drying κ-Cg is the formation of a gel between this polysaccharide and water which inhibits the diffusion of water to the surface [52]. The as-produced membrane films were denoted as $CG_xNd_z$, where C represents κ-Cg, G stands for Gly, and x and z indicate the concentrations of Gly and $NdTrif_3$, respectively, with respect to κ-Cg.

**Table 2.** Relevant details of the $CG_xNd_z$ membranes.

| $CG_xNd_z$ | | | | | |
|---|---|---|---|---|---|
| **x** | **z** | **m (κ-Cg) (g)** | **V ($H_2O$) (mL)** | **% Nd/κ-Cg** | **m (NdTrif) (g)** |
| 50 | 0 | 0.3017 | | - | - |
| | 10 | 0.3013 | | 10 | 0.0316 |
| | 20 | 0.3020 | 15 | 20 | 0.0615 |
| | 30 | 0.3006 | | 30 | 0.0919 |
| | 40 | 0.3020 | | 40 | 0.1211 |

### *3.3. Characterization Techniques*

The X-ray diffraction (XRD) measurements were recorded at room temperature with a Rigaku Dmax III/C X-ray diffractometer, power 40 kV/30 mA and using monochromated $CuK_\alpha$ radiation (λ = 1.5418 Å) over the 2θ range of 10 to 70.0° at 1.2° $min^{-1}$.

DSC curves of the samples were recorded using a Netzsch instrument (model STA 449 F3 Jupiter, Nurnberg, Germany). The samples were transferred to aluminum crucibles, covered with pin holed seals, and then heated from 30 to 260 °C at 10 °C $min^{-1}$. Dry nitrogen was used as purge and protective gases (50 mL $min^{-1}$).

Scanning electron microscopy (SEM) images were obtained at 20 kV on a Hitachi S-3400N type II microscope equipped with a Bruker x-flash 5010 at high vacuum. The sample was coated with gold. Elemental mapping of the samples was performed by Energy Dispersive X-ray (EDX) analysis. The acquisition time for a satisfactory resolution and noise performance was 30 s.

The Fourier Transform Raman (FT-Raman) spectra were recorded at room temperature with an FT Raman Bruker RFS 100/S spectrometer equipped (Hamburg, Germany) with a Nd-YAG with wavelength 1064 nm (350 mW). The spectra were collected over the 4000–100 $cm^{-1}$ range by averaging 1500 scans at a resolution of 4 $cm^{-1}$.

To evaluate complex FT-Raman band envelopes and to identify underlying spectral components, the iterative least-squares curve-fitting procedure in the PeakFit software (version 4) [53] was used extensively. The best fit of the experimental data was obtained by varying the frequency, bandwidth, and intensity of the bands. As the morphology of the materials was under investigation, Gaussian band shapes were employed. A linear baseline correction with a tolerance of 0.2% was used. The standard errors of the curve-fitting procedure were less than 0.0002.

Bulk ionic conductivities ($\sigma_i$) of the membranes were obtained during heating cycles from room temperature to 60 °C, over the frequency range of 65 kHz to 0.5 Hz, by means of an Autolab PGSTAT-12 (Eco Chemie, Utrecht, The Netherlands), and using cell GE/electrolyte membrane/GE (where GE stands for 10 mm diameter ion-blocking gold electrodes, Goodfellow, > 99.95%). Prior to characterization, the κ-Cg based electrolytes were vacuum-dried at 50 °C for about 48 h and stored in an argon-filled glovebox. The electrode–membrane–electrode assembly was secured in a suitable constant-volume support, which was installed in a Buchi TO 51 tube oven. A calibrated type-K thermocouple placed close to the membrane disc was used to measure the sample temperature with a precision of about 0.2 °C. The $CG_xNd_z$ electrolytes demonstrated almost ideal semiconductor behavior up to 60 °C and bulk conductivities were extracted in the conventional manner from impedance data by using an equivalent circuit composed of $R_b$ in parallel with $G_c$, where $R_b$ is the bulk electrical resistance of the electrolyte and $G_c$ is its geometric capacity. The circuit element corresponding to the blocking electrode interface was simulated by a series $C_{dl}$ elements, where $C_{dl}$ is the double layer capacity. The $\sigma_i$ was calculated using the expression,

$$\sigma i = d/(R_b\ A) \quad (1)$$

where $R_b$, $d$ and $A$ are the bulk resistance, the thickness and the area of the electrolyte sample, respectively.

The emission and excitation spectra were recorded using a Fluorolog3® Horiba Scientific (Model FL3-2T, Montpellier, France) spectroscope, with a modular double grating excitation spectrometer (fitted with a 1200 grooves/mm grating blazed at 330 nm) and a TRIAX 320 single emission monochromator (fitted with a 1200 grooves/mm grating blazed at 500 nm, reciprocal linear density of 2.6 nm $mm^{-1}$), coupled to R928 (UV/visible measurements) or H10330A (NIR measurements) Hamamatsu photomultiplier, using the front face acquisition mode. The excitation source was a 450 W Xe arc lamp. The emission spectra were corrected for detection and optical spectral response of the spectrofluorimeter and the excitation spectra were corrected for the spectral distribution of the lamp intensity using a photodiode reference detector. Moreover, a band path filter was used to avoid stray radiation arising from the monitoring wavelength in the excitation spectra.

## 4. Conclusions

SPEs consisting of a κ-Cg, $NdTrif_3$, and Gly were prepared via solvent-casting. In the present work, we have reported structural, morphological and optical properties, thermal behavior, ionic conductivity, and the degree of ionic associations of membranes, as a function the $NdTrif_3$ content. The analysed membranes show a semi-crystalline nature, with predominance of amorphous phase and a homogeneous, non-rough texture with small spherical micro-aggregates. A maximum ionic conductivity was achieved in an optimized sample with 50 wt.% Gly/κ-Cg and 20 wt.% $NdTrif_3$/κ-Cg, ($1.03 \times 10^{-4}$, $3.03 \times 10^{-4}$, and $1.69 \times 10^{-4}$ S $cm^{-1}$ at 30, 60, and 97 °C, respectively). FT-Raman spectroscopy suggests that the charge carriers of membrane with highest conductivity are "free" $Trif^-$ ions or weakly coordinated species. The $NdTrif_3$-based κ-Cg membranes present UV/visible and NIR emission associated with the κ-Cg based host and the $Nd^{3+}$, $^4F_{3/2} \rightarrow {}^4I_{11/2\text{-}9/2}$, respectively. These membranes also display radiative energy transfer, named as "inner filter" effect. The encouraging results reported in this work suggest that similar electrolytes incorporating highly efficient $Nd^{3+}$ β-diketonate complexes instead of the salt employed here, may find application in ECDs featuring attractive attributes, such as continuous NIR emission and UV harvesting ability. These characteristics are of interest for the next generation of nearly-zero smart windows of the future sustainable buildings. These devices will help curbing the energy consumption in the building, will avoid the need for anti-UV coatings, while contributing to the increase of the occupant's well-being. Considering that the transmission of this type of polysaccharide-based electrolytes is not very high in the bleached state [30], we may further speculate that this sort of electrolytes will be suitable for anti-glare purposes.

**Supplementary Materials:** The following are available online. Figure S1: SEM images of selected $CG_{50}Nd_z$ membranes with z = 20 and 40% (b). EDS mapping images for z = 20% (a1–a6) and z = 40% (b1–b6) for Ca (calcium, purple), S (sulphur, blue), F (fluor, yellow), K (potassium, cyanide), O (oxygen, green), and Nd (neodymium, pink) atoms. Figure S2: DSC curves of selected $CG_{50}Nd_z$ membranes.

**Author Contributions:** The manuscript was written through contributions of all authors. All authors have given approval to the final version of the manuscript. Conceptualization: S.C.N. and V.d.Z.B.; synthesis of the electrolytes, characterization via DSC and FT-Raman analysis: S.M.S.; SEM measurements and organization of all data: S.C.N.; complex impedance measurements of the electrolytes: R.F.P.P. and M.M.S.; Photoluminescence measurements and discussion: L.D.C. and R.A.S.F.; writing—original draft preparation: S.C.N. and R.A.S.F.; writing—review and editing: V.d.Z.B., S.C.N. and M.C.G.; visualization: all the authors; supervision: V.d.Z.B., and M.C.G.; Validation: V.d.Z.B.; project administration and funding acquisition: V.d.Z.B.

**Funding:** This research was funded by National Funds by Foundation for Science and Technology (FCT) and by FEDER funds through the POCI-COMPETE 2020 - Operational Programme Competitiveness and Internationalisation in Axis I - Strengthening research, technological development and innovation (FCOMP-01-0124-FEDER-037271, Pest-OE/QUI/UI0616/2014 and UID/CTM/50025/2013), project LUMECD (POCI-01-0145-FEDER-016884 and PTDC/CTM-NAN/0956/2014), project UniRCell (SAICTPAC/0032/2015, POCI-01-0145-FEDER-016422)), and by the Portuguese National NMR Network (RNRMN). S. C. Nunes was funded by FCT projects (Post-PhD Fellowships of UniRCell and LUMECD projects). The R. F. P. Pereira was funded by FCT (SFRH/BPD/87759/2012 grant).

**Acknowledgments:** The authors thank CPKelco (U.S.A.) for providing the k-carrageenan sample.

**Conflicts of Interest:** The authors declare no conflict of interest.

## References


1. Sudhakar, Y.N.; Selvakumar, M.; Bhat, K. *Biopolymer Electrolytes-Fundamentals and Applications in Energy Storage*, 1st ed.; Elsevier: Amsterdam, The Netherlands, 2018.
2. Samsudin, A.S.; Khairul, W.M.; Isa, M.I.N. Characterization on the potential of carboxy methylcellulose for application as proton conducting biopolymer electrolytes. *J. Non-Cryst. Solids* **2012**, *358*, 1104–1112. [CrossRef]
3. Xu, X.; Zhou, J.; Nagaraju, D.H.; Jiang, L.; Marinov, V.R.; Lubineau, G.; Alshareef, H.N.; Oh, M. Flexible, Highly graphitized carbon aerogels based on bacterial cellulose/lignin: Catalyst-free synthesis and its application in energy storage devices. *Adv. Funct. Mater.* **2015**, *25*, 3193–3202. [CrossRef]
4. Du, X.; Zhang, Z.; Liu, W.; Deng, Y. Nanocellulose-based conductive materials and their emerging applications in energy devices—A review. *Nano Energy* **2017**, *35*, 299–320. [CrossRef]
5. Leones, R.; Fernandes, M.; Ferreira, R.A.S.; Cesarino, I.; Lima, J.F.; Carlos, L.D.; Bermudez, V.D.; Magon, C.J.; Donoso, J.P.; Silva, M.M.; et al. Luminescent DNA- and Agar-based membranes. *J. Nanosci. Nanotechnol.* **2014**, *14*, 6685–6691. [CrossRef] [PubMed]
6. Firmino, A.; Grote, J.G.; Kajzar, F.; M'Peko, J.-C.; Pawlicka, A. DNA-based ionic conducting membranes. *J. Appl. Phys.* **2011**, *110*, 033704–033709. [CrossRef]
7. Avellaneda, C.O.; Vieira, D.F.; Al-Kahlout, A.; Heusing, S.; Leite, E.R.; Pawlicka, A.; Aegerter, M.A. All solid-state electrochromic devices with gelatin-based electrolyte. *Sol. Energy Mater. Sol. Cells* **2008**, *92*, 228–233. [CrossRef]
8. Ramadan, R.; Kamal, H.; Hashem, H.M.; Abdel-Hady, K. Gelatin-based solid electrolyte releasing $Li^+$ for smart window applications. *Sol. Energy Mater. Sol. Cells* **2014**, *127*, 147–156. [CrossRef]
9. Vieira, D.F.; Avellaneda, C.O.; Pawlicka, A. Conductivity study of a gelatin-based polymer electrolyte. *Electrochim. Acta* **2007**, *53*, 1404–1408. [CrossRef]
10. Alves, R.; Sentanin, F.; Sabadini, R.; Fernandes, M.; Bermudez, V.; Pawlicka, A.; Silva, M. Samarium (III) triflate-doped chitosan electrolyte for solid state electrochromic devices. *Electrochim. Acta* **2018**, *267*, 51–62. [CrossRef]
11. Alves, R.; Sentanin, F.; Sabadini, R.C.; Pawlicka, A.; Silva, M.M. Innovative electrolytes based on chitosan and thulium for solid state applications: Synthesis, structural, and thermal characterization. *J. Electroanal. Chem.* **2017**, *788*, 156–164. [CrossRef]
12. Liew, C.-W.; Ramesh, S. Studies on ionic liquid-based corn starch biopolymer electrolytes coupling with high ionic transport number. *Cellulose* **2013**, *20*, 3227–3237. [CrossRef]
13. Shukur, M.F.; Kadir, M.F.Z. Electrical and transport properties of $NH_4Br$-doped cornstarch-based solid biopolymer electrolyte. *Ionics* **2015**, *21*, 111–124. [CrossRef]
14. Raphael, E.; Avellaneda, C.O.; Aegerter, M.A.; Silva, M.M.; Pawlicka, A. Agar-based gel electrolyte for electrochromic device application. *Mol. Cryst. Liq. Cryst.* **2012**, *554*, 264–272. [CrossRef]
15. Lima, E.; Raphael, E.; Sentanin, F.; Rodrigues, L.C.; Ferreira, R.A.S.; Carlos, L.D.; Silva, M.M.; Pawlicka, A. Photoluminescent polymer electrolyte based on agar and containing europium picrate for electrochemical devices. *Mater. Sci. Eng. B* **2012**, *177*, 488–493. [CrossRef]
16. Tavares, F.C.; Dörr, D.S.; Pawlicka, A.; Oropesa Avellaneda, C. Microbial origin xanthan gum-based solid polymer electrolytes. *J. Appl. Polym. Sci.* **2018**, *135*, 46229–46234. [CrossRef]
17. Pereira, R.F.P.; Sentanin, F.; Pawlicka, A.; Goncalves, M.C.; Silva, M.M.; Bermudez, V.D. Smart windows prepared from Bombyx mori Silk. *Chemelectrochem* **2016**, *3*, 1084–1097. [CrossRef]
18. Nunes, S.C.; Pereira, R.F.P.; Sousa, N.; Silva, M.M.; Almeida, P.; Figueiredo, F.M.L.; de Zea Bermudez, V. Eco-friendly red seaweed-derived electrolytes for electrochemical devices. *Adv. Sustain. Syst.* **2017**, *1*, 1700070. [CrossRef]
19. Silva, M.M.; Bermudez, V.d.Z.; Pawlicka, A. Application of Polymer Electrolytes for Electrochemical Devices. In *Polymer Electrolytes: Characterization and Applications*; Winie, T., Arof, A.K., Thomas, S., Eds.; Wiley-VCH: Weinheim, Germany, 2019; Volume 2.
20. Singh, R.; Jadhav, N.A.; Majumder, S.; Bhattacharya, B.; Singh, P.K. Novel biopolymer gel electrolyte for dye-sensitized solar cell application. *Carbohydr. Polym.* **2013**, *91*, 682–685. [CrossRef]
21. Bella, F.; Mobarak, N.N.; Jumaah, F.N.; Ahmad, A. From seaweeds to biopolymeric electrolytes for third generation solar cells: An intriguing approach. *Electrochim. Acta* **2015**, *151*, 306–311. [CrossRef]

22. Ma, J.; Sahai, Y. Chitosan biopolymer for fuel cell applications. *Carbohydr. Polym.* **2013**, *92*, 955–975. [CrossRef]
23. Boopathi, G.; Pugalendhi, S.; Selvasekarapandian, S.; Premalatha, M.; Monisha, S.; Aristatil, G. Development of proton conducting biopolymer membrane based on agar–agar for fuel cell. *Ionics* **2017**, *23*, 2781–2790. [CrossRef]
24. Christopher Selvin, P.; Perumal, P.; Selvasekarapandian, S.; Monisha, S.; Boopathi, G.; Leena Chandra, M.V. Study of proton-conducting polymer electrolyte based on k-carrageenan and $NH_4SCN$ for electrochemical devices. *Ionics* **2018**, *24*, 3535–3542. [CrossRef]
25. Mobarak, N.N.; Ramli, N.; Ahmad, A.; Rahman, M.Y.A. Chemical interaction and conductivity of carboxymethyl κ-carrageenan based green polymer electrolyte. *Solid State Ionics* **2012**, *224*, 51–57. [CrossRef]
26. Rudhziah, S.; Ahmad, A.; Ahmad, I.; Mohamed, N.S. Biopolymer electrolytes based on blend of kappa-carrageenan and cellulose derivatives for potential application in dye sensitized solar cell. *Electrochim. Acta* **2015**, *175*, 162–168. [CrossRef]
27. Mobarak, N.N.; Jumaah, F.N.; Ghani, M.A.; Abdullah, M.P.; Ahmad, A. Carboxymethyl carrageenan based biopolymer electrolytes. *Electrochim. Acta* **2015**, *175*, 224–231. [CrossRef]
28. Moniha, V.; Alagar, M.; Selvasekarapandian, S.; Sundaresan, B.; Hemalatha, R.; Boopathi, G. Synthesis and characterization of bio-polymer electrolyte based on iota-carrageenan with ammonium thiocyanate and its applications. *J. Solid State Electr.* **2018**, *22*, 3209–3223. [CrossRef]
29. Jumaah, F.N.; Mobaraka, N.N.; Ahmad, A.; Ramli, N. Characterization of τ -carrageenan and its derivative based green polymer electrolytes. *AIP Conf. Proc.* **2013**, *1571*, 768–774.
30. Nunes, S.C.; Saraiva, S.M.; Pereira, R.F.P.; Pereira, S.; Silva, M.M.; Carlos, L.D.; Fortunato, E.; Ferreira, R.A.S.; Rego, R.; de Zea Bermudez, V. Sustainable dual-mode smart windows for energy-efficient buildings. *ACS Appl. Energy Mater.* **2019**. [CrossRef]
31. Liew, J.W.Y.; Loh, K.S.; Ahmad, A.; Lim, K.L.; Wan Daud, W.R. Effect of modified natural filler o-methylene phosphonic κ-carrageenan on chitosan-based polymer electrolytes. *Energies* **2018**, *11*, 1910. [CrossRef]
32. Kariduraganavar, M.Y.; Kittur, A.A.; Kamble, R.R. Chapter 1—Polymer Synthesis and Processing. In *Natural and Synthetic Biomedical Polymers*; Kumbar, S.G., Laurencin, C.T., Deng, M., Eds.; Elsevier: Oxford, UK, 2014; pp. 1–31.
33. Tanaka, F. Thermoreversible gelation strongly coupled to polymer conformational transition. *Macromolecules* **2000**, *33*, 4249–4263. [CrossRef]
34. Tanaka, F. Thermoreversible gelation driven by coil-to-helix transition of polymers. *Macromolecules* **2003**, *36*, 5392–5405. [CrossRef]
35. Mihaila, S.M.; Gaharwar, A.K.; Reis, R.L.; Marques, A.P.; Gomes, M.E.; Khademhosseini, A. Photocrosslinkable kappa-carrageenan hydrogels for tissue engineering applications. *Adv. Healthc. Mater.* **2013**, *2*, 895–907. [CrossRef]
36. Chronakis, I.S.; Doublier, J.-L.; Piculell, L. Viscoelastic properties for kappa- and iota-carrageenan in aqueous NaI from the liquid-like to the solid-like behaviour. *Int. J. Biol. Macromol.* **2000**, *28*, 1–14. [CrossRef]
37. Carrageenans. *Thermoreversible Networks: Viscoelastic Properties and Structure of Gels*; Springer: Berlin/Heidelberg, Germany, 1997; pp. 203–218.
38. Gonçalves, A.R.; da Silva, C.J.R.; Silva, M.M.; Smith, M.J. Ionic conduction and thermal properties of poly(ethylene oxide) - Er $(CF_3SO_3)_3$ films. *Ionics* **1995**, *1*, 342–347. [CrossRef]
39. de Zea Bermudez, V.; Carlos, L.D.; Duarte, M.C.; Silva, M.M.; Silva, C.J.R.; Smith, M.J.; Assunção, M.; Alcácer, L. A novel class of luminescent polymers obtained by the sol–gel approach. *J. Alloys Compd.* **1998**, *275–277*, 21–26. [CrossRef]
40. Silva, M.M.; de Zea Bermudez, V.; Carlos, L.D.; Smith, M.J. Neodymium doped, sol-gel processed polymer electrolytes. *Ionics* **1998**, *4*, 170–174. [CrossRef]
41. Pekcan, Ö.; Tari, Ö. *A Fluorescence Study on the Gel-to-Sol Transition of κ-Carrageenan*; Elselvier: Amsterdam, The Netherlands, 2004; Volume 34, pp. 223–231.
42. Nishinari, K.; Koide, S.; Ogino, K. On the temperature dependence of elasticity of thermo-reversible gels. *J. Phys. Fr.* **1985**, *46*, 793–797. [CrossRef]
43. Prasad, K.; Kaneko, Y.; Kadokawa, J.-i. Novel gelling systems of κ-, ι- and λ-carrageenans and their composite gels with cellulose using ionic liquid. *Macromol. Biosci.* **2009**, *9*, 376–382. [CrossRef]

44. Anderson, N.S.; Campbell, J.W.; Harding, M.M.; Rees, D.A.; Samuel, J.W.B. X-ray diffraction studies of polysaccharide sulphates: Double helix models for κ- and ι-carrageenans. *J. Mol. Biol.* **1969**, *45*, 85–97. [CrossRef]
45. Pradhan, D.K.; Choudhary, R.N.P.; Samantaray, B.K. Studies of dielectric relaxation and AC conductivity behavior of plasticized polymer nanocomposite electrolytes. *Int. J. Electrochem. Sci.* **2008**, *3*, 597–608.
46. Tsutsumi, H.; Matsuo, A.; Onimura, K.; Oishi, T. Conductivity enhancement of a polyacrylonitrile-based polymer electrolyte containing cascade nitrile as a plasticizer. *Electrochem. Solid State Lett.* **1998**, *1*, 244–245. [CrossRef]
47. Fujishima, M.; Matsuo, Y.; Takatori, H.; Uchida, K. Proton-conductive acid–base complex consisting of κ-carrageenan and 2-mercaptoimidazole. *Electrochem. Commun.* **2008**, *10*, 1482–1485. [CrossRef]
48. de Zea Bermudez, V.; Ostrovskii, D.; Lavoryk, S.; Cristina Gonçalves, M.; Carlos, L.D. Urethane cross-linked poly(oxyethylene)/siliceous nanohybrids doped with $Eu^{3+}$ ions Part 2. Ionic association. *Phys. Chem. Chem. Phys.* **2004**, *6*, 649–658. [CrossRef]
49. Oza, M.D.; Meena, R.; Siddhanta, A.K. Facile synthesis of fluorescent polysaccharides: Cytosine grafted agarose and κ-carrageenan. *Carbohydr. Polym.* **2012**, *87*, 1971–1979. [CrossRef]
50. Molina, C.; Ferreira, R.A.S.; Poirier, G.; Fu, L.; Ribeiro, S.J.L.; Messsaddeq, Y.; Carlos, L.D. $Er^{3+}$-Based Diureasil Organic–Inorganic Hybrids. *J. Phys. Chem. C* **2008**, *112*, 19346–19352. [CrossRef]
51. GENU®. *Carrageenan Book*; CPKelco ApS: Copenhagen, Denmark, 2001.
52. Djaeni, M.; Prasetyaningrum, A.; Sasongko, S.B.; Widayat, W.; Hii, C.L. Application of foam-mat drying with egg white for carrageenan: drying rate and product quality aspects. *J. Food Sci. Technol.* **2015**, *52*, 1170–1175. [CrossRef]
53. *Peakfit, (Version 4.0)*; SYSTAT Software Inc.: San Jose, CA, USA, 2007.


**Sample Availability:** Samples of the compounds are not available from the authors.